
The Ikshana Hypothesis of Human Scene Understanding Mechanism

Venkata Satya Sai Ajay Daliparthi
 Blekinge Institute of Technology
 Karlskrona, Sweden
 veda18@student.bth.se

Abstract

In recent years, deep neural networks (DNNs) achieved state-of-the-art performance on several computer vision tasks. However, the one typical drawback of these DNNs is the requirement of massive labeled data. Even though few-shot learning methods address this problem, they often use techniques such as meta-learning and metric-learning on top of the existing methods. In this work, we address this problem from a neuroscience perspective by proposing a hypothesis named Ikshana, which is supported by several findings in neuroscience. Our hypothesis approximates the refining process of conceptual gist in the human brain while understanding a natural scene/image. While our hypothesis holds no particular novelty in neuroscience, it provides a novel perspective for designing DNNs for vision tasks. By following the Ikshana hypothesis, we propose a novel neural-inspired CNN architecture named IkshanaNet. The empirical results demonstrate the effectiveness of our method by outperforming several baselines on the entire and subsets of the Cityscapes and the CamVid semantic segmentation benchmarks.

1 Introduction

The human brain can seamlessly perceive diverse perceptual and semantic information regarding the natural scene/image during a glance [1–4]. The visual scene information perceived during/after a glance refers to the gist (a summary) of the scene/image. The gist includes all the visual information from the low-level (e.g., colors and contours) to the high-level (e.g., shapes and activation). Due to this reason, [5] suggested that the gist can be investigated at both the perceptual and conceptual levels. The structural representation of the image refers to the perceptual gist, and the semantic information of the image refers to the conceptual gist. However, the conceptual gist is more refined and modified than the perceptual gist [5]. Several works [6, 7, 4, 8–11] in neuroscience have addressed the fundamental question, i.e., “how does the human brain performs several visual tasks?” by investigating through conceptual and perceptual gist. They conducted several experiments and proposed various theories to explain how modeling of the scene occurs in the human brain. However, there was no general principle that explains the functioning of the human brain. Even though there is a general principle, we expect that to be different from human-to-human. Depending on the situation and the environment, the human brain can seamlessly grasp the information by recognizing the objects and observing their structure. On the other hand, for a computer to do the same is the fundamental goal of the computer vision field.

In recent years, deep learning methods have shown a significant improvement over traditional handcrafted techniques on several computer vision tasks. Though these deep neural networks (DNNs) achieved state-of-the-art performance in many cases, the one major drawback is the requirement of massive labeled data. The collection of a huge amount of labeled data is an expensive and time taking process. Even though these DNNs are said to be inspired by the functioning of the human brain, is this how the human brain learns to perform any visual task? NO. Because the human brain does not

require massive labeled data to perform any visual task, and it can perform with few data samples. However, we cannot observe a similar phenomenon in the case of many DNNs.

Semantic segmentation is the task of assigning a class label to every pixel in the given image, which has applications in various fields such as medical, autonomous driving, robotic navigation, localization, and scene understanding. The prominent work FCN [12] adopted the image-classification networks [13–15] for semantic segmentation. Later on, several works [16–23] improved the FCN [12] architecture, and proven to be successful in diverse semantic segmentation benchmarks [24–26]. However, these methods mainly focus on achieving state-of-the-art performance by using the entire and additional datasets [27] (for pre-training). Even though various methods outperformed U-Net [16] in terms of accuracy and computational complexity, the U-Net [16] architecture is still exploited in several medical image segmentation methods due to its ability to perform with few data samples [28]. Several few-shot semantic segmentation (FSS) methods are introduced to address this problem. However, they often use techniques such as meta-learning [29–33] and metric learning [34–38, 38–40], on top of the FCN [12] based architectures.

Unlike FSS methods, we tackle the formerly mentioned drawback of the DNNs, i.e., the requirement of massive labeled data, from a neuroscience perspective. In this work, we propose a hypothesis of human scene understanding mechanism named Ikshana. The idea is that, “to understand the conceptual gist of a given image; humans look at the image multiple times recurrently at different scales”. Following the Ikshana hypothesis, we propose a novel neural-inspired CNN architecture named IkshanaNet, a multi-scale architecture that learns representations at full image resolution. In contrast to the existing CNN architectures that pass the input image only to the initial layer (stem module), our method feeds the input image to every module in the network.

To evaluate the performance of IkshanaNet, we conduct extensive experiments on the entire and subsets of the Cityscapes and Camvid benchmarks. Moreover, we conduct multiple ablation studies to verify the effect of image scales in IkshanaNet. The empirical results illustrate that our method outperforms several baselines on the entire and few data samples. Furthermore, the ablation studies show that IkshanaNet requires more than one image scale to achieve considerable performance.

2 Related work

2.1 Neuroscience

In Neurological terms, all the low-level and high-level computer vision tasks come under a single term called human scene understanding. A scene is a view of a real-world environment that contains multiple surfaces and objects organized in a meaningful way. In neuroscience, the perceptual gist is more investigated compared to the conceptual gist. The early works on the conceptual gist [41, 3] explained that a typical scene fixation of 275 to 300 *ms* is often sufficient to understand the gist of the image. Several works on the perceptual gist [7, 6, 42, 43, 8, 4, 9–11] provided insight into how the modelling of the scene occurs in the human brain through perceiving boundaries, blobs, scales, texture, contours, openness, depth, and so on. The information perceived through the perceptual gist is refined and extracted into the conceptual gist (the semantic meaning) during the cognitive process. Thus, the conceptual gist is highly dependent upon the perceptual gist.

In many cases [27, 25, 26], we do not explicitly encode the perceptual process in DNNs, and the CNN learns various representations regarding the image during the training process. Thus, our hypothesis focuses on the conceptual gist rather than the perceptual gist.

2.2 Deep Learning

Neural networks exist from a long time [44–46] and some prominent works [27, 13, 47, 14, 15, 48–50] made them popular during recent years. In our work, we use the convolutional neural network (CNN) architecture [51, 52] to learn representations from the images, which itself is inspired by [53, 54]. The architecture of IkshanaNet is inspired by [14, 55] and related to [56, 57].

2.3 Semantic segmentation

The first seminal work on Semantic segmentation (SS) using deep learning is the fully convolutional networks (FCN) [12]. Later on, many semantic segmentation networks followed the FCN [12] architecture. The total prominent works on deep learning-based semantic segmentation methods can be roughly classified into five categories. They are (i) Encoder-decoder based methods (DeconvNet

[58], SegNet [17], U-Net [16], RefineNet [59, 60], FC-DenseNet [61], and GFR-Net [62]), (ii) Regional proposal methods (MaskRCNN [63], FPN [64], and PANet [65]), (iii) Increased resolution of feature map methods (DeepLab series [66–68, 19], PSPNet [18], DenseASPP [69], and HRNet [20]), (iv) Context information methods (ParseNet [70], ATS [71], DANet [72], OCNet [73], OCR [21], EncNet [74], Non-local [75], ZigZagNet [76], ACFNet [77], CoCurNet [78], GLAD [79], and HANet [80]) (v) Boundary refinement methods ([81–84], Gated-SCNN [22], and SegFix [23]). The IkshanaNet uses the dilated convolutions, interpolation of feature maps, and skip connections from different layers in the network. Therefore, our work is related to the formerly mentioned encoder-decoder and increased resolution of feature map methods.

2.4 Few-shot segmentation

Few-shot segmentation (FSS) methods [29–40, 85–87] are introduced to handle limited training data. They use meta-learning (knowledge distillation), metric-learning (similarity learning), and a combination of both the techniques on top of FCN [12] based architectures, which often involve multistage training. The metric-learning techniques can be further classified into the prototypical feature learning [30, 88, 36, 37, 35, 89] and the affinity learning [38, 39, 90] techniques. Unlike general SS methods, FSS methods are evaluated on different benchmarks and handle novel class categories during testing. Since the IkshanaNet does not use any of the formerly mentioned FSS techniques and only handles the classes seen in the training data, our method is more closely related to the general SS methods than the FSS methods.

3 Method

3.1 Ikshana (the eye) hypothesis

In her prominent work [41], professor Mary C. Potter found that an average human can understand the gist of the image between the time interval of 125 to 300 *ms*. Furthermore, through several works [3, 6, 42, 8, 4, 9–11] in neuroscience, it is evident that humans understand the gist of the image in a certain time interval. During that time interval, the Ikshana hypothesis approximates the functioning of the human brain. The Ikshana hypothesis states that **“To understand the conceptual gist of a given image, humans look at the image multiple times recurrently, at different scales.”** The word Ikshana is derived from the Sanskrit language, which has many synonyms such as the eye, sight, look, and so on.

We present an example to explain the Ikshana hypothesis in Figure 1, where there is an image (x) on the left side and the human brain mechanism on the right side. According to the Ikshana hypothesis, for a human to understand the conceptual gist of the given image, the following process occurs in the human brain:

At a time step (t), during the first glance (Φ_1), the brain learns the first representation ($f(x)$) from the image (x) and stores that representation in the memory (M), as shown in the equation 1.

$$f(x) = \Phi_1(x); \quad M = f(x) \quad (1)$$

At a time step ($t + 1$), during the second glance (Φ_2), the brain holds the first representation ($f(x)$) in the memory and learns the second representation ($g(x)$) from the image and the first representation ($x, f(x)$). Then the brain stores the representation ($g(x)$) along with ($f(x)$) in the memory (M), as shown in the equation 2.

$$g(x) = \Phi_2(x, f(x)); \quad M = f(x), g(x) \quad (2)$$

At a time step ($t + 2$), during the third glance (Φ_3), the brain holds the first and the second representations ($f(x), g(x)$) in the memory and learns the third representation ($h(x)$) from the image and the previous representations ($x, f(x), g(x)$). Then the brain stores the representation ($h(x)$) along with ($f(x), g(x)$) in the memory (M), as shown in the equation 3.

$$h(x) = \Phi_3(x, f(x), g(x)); \quad M = f(x), g(x), h(x) \quad (3)$$

From 1, 2, and 3, this kind of recurrent process occurs at ($t + n$) times at a single image scale. Depending upon the given task (T), by combing all the information stored in the memory until the ($t + n$)th time step, the brain understands the conceptual gist (Y_1) of the image at a single scale, as shown in the equation 4.

$$Y_1 = T(f(x), g(x), h(x), \dots, n(x)) \quad (4)$$

This process occurs at N different scales and generates N different outputs ($Y_1, Y_2, Y_3, \dots, Y_n$). By considering all the outputs, the brain selects some of those representations and forgets the remaining representations. In this way, the brain learns (Δ) the final output (Y) of the given visual task (T), as shown in the equation 5.

$$Y = \Delta(Y_1, Y_2, Y_3, \dots, Y_n) \quad (5)$$

From the equations 1, 2, 3, 4, and 5, this is how Ikshana hypothesis approximates the functioning of the human brain, while human understands the conceptual gist of the image. The time required (or the number of glances required) by an average human to understand the gist of the image may depend upon several factors such as the given task, age, intelligence, memory, and so on.

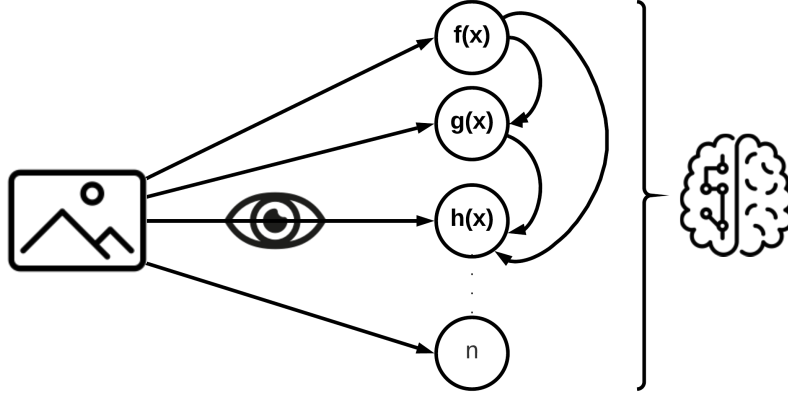


Figure 1: The Ikshana hypothesis at single scale

The existing CNN architectures such as VGG [14], Resnet [48], DenseNet [55], and so on learn a representation (say $f(x)$) with 32/64 filters from the input image and learn further representations on top of the $f(x)$ until the network achieves adequate performance. In contrast, the network designed by following the Ikshana hypothesis learns representations from the input image and previous outputs at each glance/layer.

3.2 IkshanaNet-main

In this section, we introduce a novel neural-inspired encoder-decoder CNN architecture named IkshanaNet, designed by following the Ikshana hypothesis. Humans can look at the image and seamlessly learn various useful representations regarding it [1–4]. On the other hand, for a computer to do the same, we use the convolutional neural network [53, 54, 51] architecture to learn representations. The IkshanaNet architecture uses three image scales and consists of 4M parameters. The entire architecture is made of three building blocks, and they are: (1) the glance module, (2) the projection module, and (3) a 1×1 convolutional layer, shown in Figure 2.

The **glance module** consists of three 3×3 convolutional layers (with the same dilation rates), and we use it to learn representations from the given image (or a feature map).

The number of input filters passed into the glance module varies several times in the architecture; however, it always returns a feature map with 32 filters.

The **projection module** consists of three 3×3 convolutional layers, and we use it to refine the representations learned from the glance modules. The input and output filters are always the same for the projection module.

We use the **1×1 convolution layers** to reduce the number of filters in a given feature map. Except for the last 1×1 convolutional layer that returns the final output, every convolutional layer in the architecture is followed by a batch normalization [91] and a ReLU [92] activation layer.

In the **encoder** part, the IkshanaNet learns representations at three image scales. At scale 1, we pass the input image through a glance module with a dilation rate ($d=1$), which returns a feature map with 32 filters. Then we concatenate the input image with the previously learned feature map ($32 + 3 = 35$). The concatenation of the input image in the feature map is essential to ensure that we are learning representations from the input image. Then we pass the feature map through

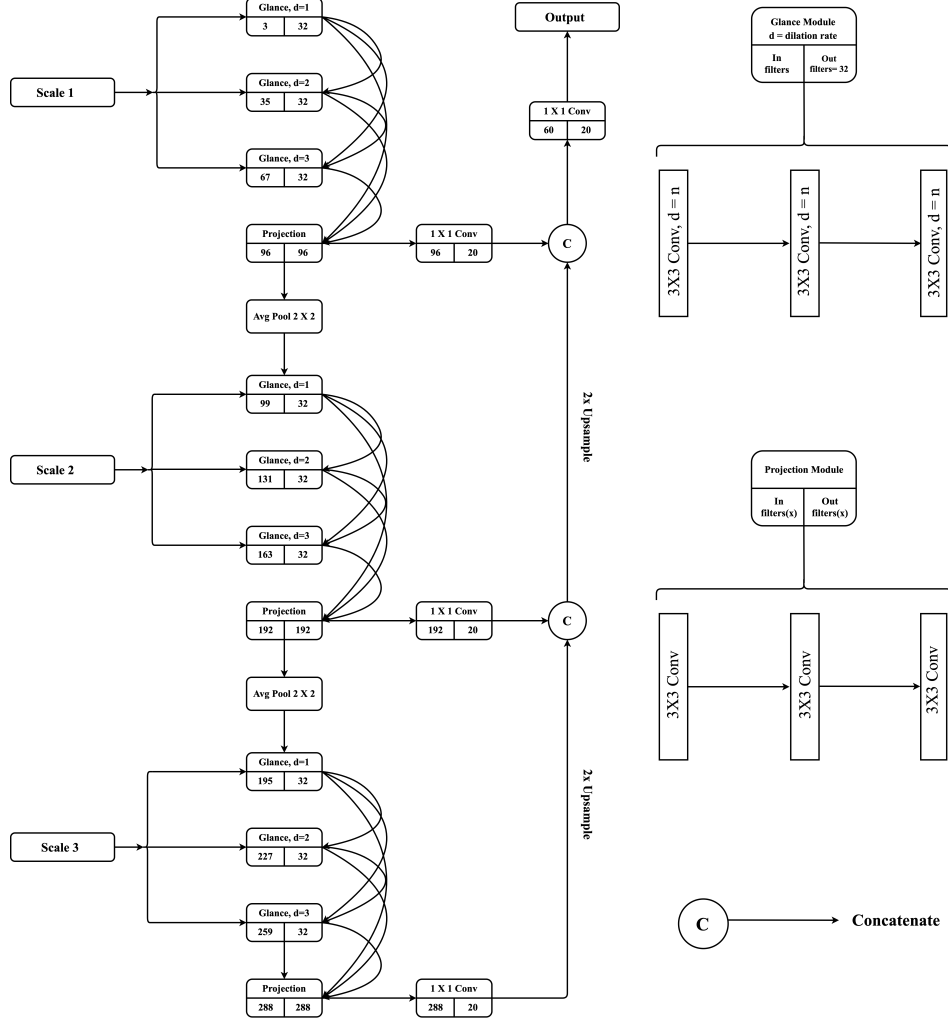


Figure 2: IkshanaNet-main architecture

another glance module with a dilation rate ($d=2$) and concatenate the resulting feature map with the feature maps from the preceding layers ($32 + 32 + 3 = 67$). We pass the resulting feature map through another glance module with a dilation rate ($d=3$), which takes in 67 filters and returns 32 filters. Again, we concatenate the resulting feature map with feature maps from the preceding layers ($32 + 32 + 32 + 3 = 99$). At this point, we remove the input image from the feature map through tensor slicing ($99 - 3 = 96$), and the resulting feature map consists of ($32 + 32 + 32 = 96$) filters learned from three glances modules. In this way, the network followed the Ikshana hypothesis and had three glances recurrently at the full resolution. Then we pass the feature map through a projection module to refine the representations ($96 = 96$). Here, we pass the refined feature map through a 1×1 convolutional layer that reduces 96 filters into 20 filters and name it the side one output (Y_1). Simultaneously, we pass the feature map through an average pooling layer, which reduces the size of the feature map by a factor of two.

At scale 2, we down-sample the input image by a factor of two and concatenate with the pooled feature map from the scale 1 ($96 + 3 = 99$). We pass the resulting feature map with 99 filters through three glance modules with different dilation rates ($d=1, 2, 3$) and concatenate all the outputs as follows ($99 + 32 + 32 + 32 = 195$). Then we remove the image from the feature map ($195 - 3 = 192$) and pass it through a projection module to refine the representations ($192 = 192$). Then we pass the refined feature map through a 1×1 convolutional layer that reduces 192 filters into 20 filters and name it the side two output (Y_2). Then, we pass the refined feature map through an average pooling layer that reduces the size by a factor of two.

At scale 3, we down-sample the input image by a factor of four and concatenate with the pooled feature map from the scale 2 ($192 + 3 = 195$). Here, we follow the same process ($195 + 32 + 32 + 32 = 291$); ($291 - 3 = 288$); ($288 == 288$) as the scale 2 part, which returns a feature map with 20 filters, and name it the side three output (Y_3).

In the **decoder** part, we bi-linearly interpolate the outputs from two scales (Y_2 and Y_3) to match with the output of scale 1 Y_1 , i.e., the input image size. Then we concatenate all the three outputs ($20 + 20 + 20 = 60$) and pass it through a 1×1 convolutional layer, which returns a feature map with 20 filters, that is the final output of the network. [$Y = \Delta(Y_1, Y_2, Y_3)$]

Depth architectures : Here, we introduce three variants of the IkshanaNet named IkshanaNet-3G, IkshanaNet-6G, and IkshanaNet-12G. If we remove the projection layers in IkshanaNet-main, then it will remain with three scales and three glances at each scale; it is IkshanaNet-3G (which consists of 514K parameters). If we increase the number of glances per scale, from three to six, then it is IkshanaNet-6G (which consists of 1.8M parameters), and from three to twelve, then it is IkshanaNet-12G (which consists of 6.5M parameters).

Multi-scale architectures : Here, we introduce three variants of IkshanaNet named IkshanaNet-1S-6G, IkshanaNet-2S-3G, and IkshanaNet-3S-2G. In IkshanaNet-1S-6G, there are no pooling layers and contain six glances at full-scale resolution (which consists of 257K parameters). In IkshaNet-2S-3G, there are two scales and three glances at each scale (which consists of 259K parameters). In IkshanaNet-3S-2G, there are three scales and two glances at each scale (which consists of 260K parameters).

4 Experiments

4.1 Experimental setup

Framework : PyTorch 1.8 [93]

GPU: 1 X NVIDIA Tesla T-4 (16 GB VRAM)

Epochs : 180

Batch size : 2

Criterion : Pixel-wise cross-entropy loss

Learning rate scheduler : ReduceLROnPlateau (decrease factor = 0.5 and patience = 20 epochs) with an initial learning rate of $1e - 06$.

Optimizer : Stochastic gradient descent [94] with Nesterov momentum [95] ¹

Random seed : To ensure that data splits are reproducible, we set the random seed 42 in the function `torch.utils.data.random-split`.

Pre-processing We normalize all the images with mean and standard deviation values of ImageNet [27] dataset. We did not use any data augmentation techniques.

Baselines: We use the open-source implementations for networks DeepLabV3+ (ResNet-101) [99], DeepLabV3 (DenseNet-161) [100], HRNet-V2 [101], and U-Net [102]. We import DeeplabV3+ with encoder networks such as ResNet [48], MobileNet-V2 [96], ResNext [103], EfficientNet [97], and RegNet [98] from the segmentation models library [104].

4.2 Experiments on Cityscapes

The Cityscapes [25] semantic segmentation dataset consists of 5,000 finely annotated high-quality images, which are further divided into 2,975/500/1,525 images for training, validation, and testing. During the evaluation, only 19 classes are considered out of the 35 classes. Therefore, by using the cityscapes-scripts, we convert the 35 classes into 20 classes (including background). We resize all the images from the resolution of 1024x2048 to 512x1024.

¹For all the baselines, we use the Nesterov momentum of 0.9 for the SGD [94] optimizer by following [19, 55, 48, 96–98]. For the IkshanaNet and its variants, we use the Nesterov momentum of 0.7 for the SGD [94] optimizer by tuning with several values such as 0.5, 0.6, 0.7, 0.8, and 0.9, i.e., the only hyper-parameter tuning step in this work. In our preliminary experiments, we observe that the training of IkshanaNet is unstable with 0.9 momentum. We hypothesize that this phenomenon is due to the small size of IkshanaNet compared to baseline networks

4.2.1 Baseline experiments

Here, we use the networks DeeplabV3+ (ResNet-101 [48]), DeeplabV3 (DenseNet-161 [55]), HRNet-V2 [105], and U-Net [16] as the baselines² to compare with IkshanaNet-main. We train all the networks on the entire dataset T_{2975} and provide the mean class IoU results evaluated on the validation-set in Table 1, where we observe the following:

- (i) U-Net [16] (49.3) shown top performance within the baseline networks followed by HRNet-V2 [105] (48.0).
- (ii) IkshanaNet-main outperformed U-Net by 5.2 percent and HRNet-V2 [105] by 6.5 percent.
- (iii) IkshanaNet outperformed baselines by a huge margin in classes such as fence, pole, traffic light, traffic sign, rider, bus, motorcycle, and bicycle. Even though U-Net [16] and IkshanaNet learn representations at full-scale resolution before applying pooling operations, the IkshanaNet still outperforms U-Net [16] in the formerly mentioned classes.

Table 1: Class-wise results of the Cityscapes baseline experiments evaluated on the validation set

Method	road	sidewalk	building	wall	fence	pole	traffic light	traffic sign	vegetation	terrain	sky	person	rider	car	truck	bus	train	motorcycle	bicycle	Average
ResNet101 [48]	95.0	66.1	81.9	15.0	13.5	26.7	20.7	29.5	86.7	55.4	89.3	48.5	6.3	85.5	6.8	26.1	19.0	9.8	32.0	42.8
DenseNet161 [55]	94.8	64.5	81.3	20.1	13.0	15.8	15.6	28.7	84.6	58.7	86.1	44.1	0.6	84.7	17.0	19.7	23.1	4.3	31.4	41.5
HRNet-V2 [105]	94.9	68.6	84.2	24.0	24.5	39.0	23.2	42.3	86.9	51.5	90.2	55.6	15.3	86.1	19.9	36.1	21.2	2.2	46.1	48.0
U-Net [16]	94.9	69.4	85.3	27.3	28.7	41.0	32.2	49.0	88.6	46.3	90.4	59.1	14.5	86.5	12.4	28.4	15.5	10.9	55.6	49.3
IkshanaNet-Main	95.6	72.8	85.9	22.6	35.3	49.6	47.0	60.7	89.2	48.9	91.6	63.3	28.8	87.1	18.4	40.3	21.8	16.5	60.8	54.5

4.2.2 Data ablation study

While trained on few data samples, the network size might strongly influence the performance. The networks ResNet-101 [48] (59.3 M), DenseNet-161 [55] (43.2 M), HRNet-V2 [105] (65.9), and U-Net [16] (31.0) consists more number of parameters compared to IkshanaNet-main (4 M). To make it a fair comparison, we also include DeeplabV3+ [19] with several light-weight encoder networks (such as ResNet-18 [48], MobileNet-V2 [96], EfficientNet-b1 [97], and RegNetY-08 [98]) as baselines.

Here, we conduct a data ablation study on five different subsets of the training data, T_{1487} , T_{743} , T_{371} , T_{185} , and T_{92} (suffix number represents the number of training samples in the subset) by using the same validation set (500 images).

In table 2, we provide the mean class IoU results evaluated on the validation set, the average M.IoU score, the number of parameters (in million), and the GFLOPs [106] (calculated with an input resolution of $1 \times 512 \times 1024 \times 3$). From table 2, we observe the following:

- (i) U-Net [16] (T_{avg} - 32.2) achieves top average performance within the baselines
- (ii) Even though U-Net [16] consists of 31M parameters, it still managed to outperform other lightweight architectures.
- (iii) The IkshanaNet outperformed all other baselines in the M.IoU score and the average M.IoU score in all five subsets. Moreover, IkshanaNet consists of fewer parameters, and EfficientNet-b1 [97] consists of fewer GFLOPs than other networks.

4.2.3 Multi-scale ablation study

Designing a DNN by following the Ikshana hypothesis provides the flexibility to learn representations at the full-scale resolution without using any pooling operations. However, in Section 3.1, the Ikshana hypothesis stated that ‘‘humans often require multi-scale information to understand the gist of an image’’. Therefore, to verify the requirement of multi-scale information, we conduct a multi-scale ablation study. Here, we train three different variants of IkshanaNet, such as the 1S-6G, 2S-3G, and 3S-2G (explained in Section 3.2) on the five different subsets of the training data (same as Section 4.2.2).

In table 3, we provide the results of the multi-scale ablation study evaluated on the validation set. From table 3, we observe the following:

- (i) IkshanaNet-3S-2G network outperforms other networks in the M.IoU score, the average M.IoU

²For the baselines, ResNet-101 [48], DenseNet-161 [55], and HRNet-V2 [105], we use the ImageNet [27] pre-trained weights. Because in the existing literature, the architectures [19, 18, 21, 105] used an ImageNet pertained network as a feature extractor and reported the results by using pre-trained weights only. However, in the case of IkshanaNet and U-Net [16] no pre-training is done.

Table 2: Cityscapes data ablation experiments evaluated on the validation set

Backbone	T_{1487}	T_{743}	T_{371}	T_{185}	T_{92}	T_{avg}	Param(M)	GFLOPs
ResNet-18 [48]	42.6	35.6	27.9	22.4	21.0	29.9	12.3	36.8
MobileNet-V2 [96]	38.5	32.2	30.6	22.5	19.2	28.6	4.4	12.3
EfficientNet-b1 [97]	37.8	32.5	26.9	24.6	19.8	28.3	7.4	4.6
RegNetY-08 [98]	28.5	31.9	29.4	27.4	22.1	27.9	7.0	17.2
ResNet-101 [48]	29.3	28.8	28.6	21.6	19.4	25.5	59.3	177.8
DenseNet-161 [55]	33.3	30.1	26.0	24.9	20.8	27.0	43.2	129.4
HRNet-V2 [105]	27.8	18.8	23.3	18.3	15.4	20.7	65.9	187.8
U-Net[16]	42.8	34.2	30.2	27.8	25.0	32.0	31.0	387.1
IkshanaNet-Main	43.4	40.2	31.7	29.9	25.8	34.2	4.0	413.3

Table 3: Cityscapes multi-scale ablation experiments evaluated on the validation set

Backbone	T_{1487}	T_{743}	T_{371}	T_{185}	T_{92}	T_{avg}	Param(M)	GFLOPs
1S-6Glances	29.2	24.9	23.3	20.2	18.1	23.1	0.26	136.0
2S-3Glances	37.3	34.9	33.2	25.7	24.0	31.0	0.26	70.0
3S-2Glances	43.5	36.9	34.4	27.5	26.5	33.8	0.26	42.4

score, and requires fewer GFLOPs, while requiring the same number of parameters.

(ii) Using multi-scale information improves the performance and decreases the computational complexity (GFLOPs) of the networks and vice-versa.

Also, from Table 2 and Table3, we observe that IkshanaNet-3S-2G (with only 260K parameters) network outperforms all the baselines in the data ablation study by occupying approximately 10x few GFLOPs and 15x few parameters than IkshanaNet-main.

4.3 Experiments on Camvid

The Cambridge-driving labeled video dataset [24] for semantic segmentation consists of 700 images, which are further divided into 367 training, 101 validation, and 233 testing sets. We convert the 32 classes to 12 classes (including background) by following [17, 107] and resize the images from the resolution of 720x960 to 368x480.

4.3.1 Baseline experiments

Here, according to the size of the networks, we classify the total networks into three different sets.

Set-1 consists of DeeplabV3+ [19] with the encoder networks such as Resnet-18 [48], EfficientNet-b1 [97], RegNetY-08 [98], MobileNet-V2 [96], and IkshanaNet-3G (see Section 3.2).

Set-2 consists of DeeplabV3+ [19] with the encoder networks such as Resnet-50 [48], EfficientNet-b4 [97], RegNetY-40 [98], and ResNext-50 [103], and IkshanaNet-6G (see Section 3.2).

Set-3 consists of DeeplabV3+ [19] with the encoder networks such as Resnet-101 [48], EfficientNet-b6 [97], RegNetY-80 [98], DeepLabV3 (DenseNet-161 [55]), HRNet-V2 [105], U-Net [16], and IkshanaNet-12G (see section 3.2) ³.

Additionally, we include IkshanaNet-main and did not compare it with other networks. By using the same validation and the test set, we train each network on three different subsets of the training data, T_{367} , T_{183} , and T_{91} (the suffix represents the number of training samples in the subset).

In table 4, we provide the mean IoU results evaluated on the validation set, the test set, the average M.IoU score of all the variants, the number of parameters (in Million), and the GFLOPs [106] (calculated the GFLOPs with an input resolution of 1x368x480x3).

From table 4, we observe the following:

³Same as section 4.2.1, except for U-Net [16] and IkshanaNet-12G, we use the ImageNet [27] pre-trained weights for all the networks in the Set-3.

In **Set-1**:

- (i) IkshanaNet-3G outperforms other networks in the subsets T_{91} , T_{avg} , and requires fewer parameters.
- (ii) EfficientNet-b1 [97] outperforms other networks in the T_{367} and requires fewer GFLOPs.

In **Set-2**:

- (i) IkshanaNet-6G outperforms other networks in the subsets T_{367} , T_{183} , T_{avg} , and requires fewer parameters.
- (ii) EfficientNet-b4 [97] outperforms all other networks in the subset T_{91} and requires fewer GFLOPs.

In **Set-3**:

- (i) IkshanaNet-12G outperforms other networks in the subsets T_{367} , T_{183} , T_{avg} , and requires fewer parameters.
- (ii) U-Net [16] outperformed other networks in the subset T_{91} and EfficientNet-b6 [97] requires fewer GFLOPs than other networks.

Table 4: Camvid baseline experiments evaluated on the validation and the test set

Backbone	T_{367}		T_{183}		T_{91}		T_{avg}		Param(M)	GFLOPs
	Val	Test	Val	Test	Val	Test	Val	Test		
ResNet-18 [48]	83.3	64.9	79.7	63.7	70.0	56.6	77.7	61.7	12.3	12.4
EfficientNet-b1 [97]	84.4	68.4	75.0	61.3	77.0	58.8	78.8	62.8	7.4	1.5
RegNetY-08 [98]	80.4	64.3	77.7	61.4	70.9	57.8	76.3	61.2	7.0	5.8
MobileNet-V2 [96]	80.8	63.9	77.3	56.1	66.1	54.6	74.7	58.2	4.4	4.1
IkshanaNet-3G	81.6	65.7	80.0	62.5	78.0	61.2	79.9	63.1	0.5	26.0
ResNet-50 [48]	78.6	61.6	80.0	60.3	78.3	55.9	80.0	59.3	26.7	25.0
EfficientNet-b4 [97]	82.7	64.1	77.7	62.2	75.6	60.5	78.7	62.3	18.6	1.7
RegNetY-40 [98]	80.8	62.0	76.4	61.0	74.9	59.2	77.4	60.7	21.5	18.8
ResNext-50 [103]	80.1	62.6	77.3	56.1	66.1	54.6	74.5	57.8	26.2	25.0
IkshanaNet-6G	83.3	67.8	81.4	65.9	76.0	60.0	80.2	64.6	1.8	82.0
ResNet-101 [48]	81.6	63.8	75.6	56.4	70.1	55.7	75.8	58.6	59.3	59.9
EfficientNet-b6 [97]	80.6	65.0	80.3	57.8	77.4	60.4	79.4	61.0	42.0	1.9
RegNetY-80 [98]	78.5	62.0	78.2	63.8	66.2	53.8	74.3	59.9	40.3	34.4
DenseNet-161 [55]	77.8	58.6	75.7	57.8	73.0	53.8	75.5	56.7	43.2	43.6
HRNet-V2 [105]	81.1	63.6	79.1	62.9	72.9	55.0	77.7	60.5	65.9	63.5
U-Net [16]	83.0	69.5	78.0	62.8	76.8	61.6	79.3	64.6	31.0	130.0
IkshanaNet-12G	83.9	70.0	83.3	67.1	76.5	60.6	81.2	65.9	6.5	285.0
IkshanaNet-M	83.2	68.5	79.9	62.9	72.2	58.8	78.4	63.4	4.0	139.0

Table 5: Camvid multi-scale ablation experiments evaluated on the validation and the test set

Backbone	T_{367}		T_{183}		T_{91}		T_{avg}		Param(M)	GFLOPs
	Val	Test	Val	Test	Val	Test	Val	Test		
1S-6Glances	79.2	60.0	77.8	58.8	66.7	50.9	74.6	56.6	0.26	45.6
2S-3Glances	80.1	65.6	79.5	60.1	77.2	59.5	78.9	61.7	0.26	23.1
3S-2Glances	82.9	66.5	80.9	62.8	77.5	60.8	80.4	63.4	0.26	14.0

4.3.2 Multi-scale ablation study

Same as Section 4.2.3, by using the same validation and the test set, we train three different variants of IkshanaNet such as 1S-6G, 2S-3G, and 3S-2G (explained in section 3.2) on three subsets of the training data (T_{367} , T_{183} , and T_{91}).

In table 5, we provide the mean IoU results evaluated on the validation set, the test set, the average score of all variants, the parameters, and the GFLOPs. We calculate the GFLOPs with an input resolution of 1x368x480x3.

From table 5, we observe that, the IkshanaNet-3S-2G network outperforms all other networks in all the subsets (T_{367} , T_{183} , T_{91} , T_{avg}), and requires fewer GFLOPs. The results are similar to the section 4.2.3 (Table 3), demonstrating the importance of multi-scale information.

5 Validity threats

- (i) In this work, even though the training data splits are reproducible, the performance of the networks trained on subsets of the training data might depend upon the fact that “how well the subset represents the whole dataset?”. If we use a different random seed to generate the splits, then the exact behavior might not be expected.
- (ii) In this work, through multi-scale ablation experiments, we illustrate that multi-scale information is often necessary to improve the performance of the networks. By observing the images in the Cityscapes, and the CamVid datasets, it is evident that the images consist of multi-scale objects. However, this phenomenon might not be valid to other datasets, where there exist no multi-scale objects.

6 Conclusion

In this work, we attempt to bridge the gap between the current deep CNNs and the human visual system by proposing a hypothesis of human scene understanding and a novel neural-inspired CNN architecture that learns representations at full-scale resolution. The empirical results illustrate the effectiveness of our method on entire and few data samples compared to the baselines. Through multi-scale ablation studies, we observe that using multi-scale information improves the performance of IkshanaNet by reducing the computational complexity.

Moreover, we observe that our method is just an improvement over the baselines, and it is still dependent on the data. Hence, it is nowhere close to the human visual system. Therefore, a better-performing and computationally efficient architectures based on the Ikshana hypothesis will be studied in the future.

Broader Impact

Using an image classification network as a feature encoder is the most commonly observed architectural pattern in many deep learning-based computer vision techniques. Our method might provide people with an additional encoder network to consider, especially to deal with the high-level computer vision tasks, where the spatial location plays a crucial role in the final output. The one key challenge faced by the people who are working on the few-shot learning through meta-learning paradigm is that the base network over-fits the training data due to the massive number of parameters [108]. Since the IkshanaNet-3S-2G (see 3.2) network consists of only 260K parameters, using our network as a base learner might help mitigate the risk of overfitting the data.

References

- [1] Alinda Friedman. Framing pictures: The role of knowledge in automatized encoding and memory for gist. *Journal of experimental psychology: General*, 108(3):316, 1979.
- [2] Mary C Potter. Short-term conceptual memory for pictures. *Journal of experimental psychology: human learning and memory*, 2(5):509, 1976.
- [3] Helene Intraub. Rapid conceptual identification of sequentially presented pictures. *Journal of Experimental Psychology: Human Perception and Performance*, 7(3):604, 1981.
- [4] Aude Oliva and Antonio Torralba. Modeling the shape of the scene: A holistic representation of the spatial envelope. *International journal of computer vision*, 42(3):145–175, 2001.
- [5] Aude Oliva. Gist of the scene. In *Neurobiology of attention*, pages 251–256. Elsevier, 2005.
- [6] Keith Rayner. Eye movements in reading and information processing: 20 years of research. *Psychological bulletin*, 124(3):372, 1998.
- [7] Irving Biederman. Recognition-by-components: a theory of human image understanding. *Psychological review*, 94(2):115, 1987.
- [8] Aude Oliva and Philippe G Schyns. Diagnostic colors mediate scene recognition. *Cognitive psychology*, 41(2):176–210, 2000.

- [9] John M Henderson. Human gaze control during real-world scene perception. *Trends in cognitive sciences*, 7(11):498–504, 2003.
- [10] Karla K Evans and Anne Treisman. Perception of objects in natural scenes: is it really attention free? *Journal of Experimental Psychology: Human Perception and Performance*, 31(6):1476, 2005.
- [11] Li Fei-Fei, Asha Iyer, Christof Koch, and Pietro Perona. What do we perceive in a glance of a real-world scene? *Journal of vision*, 7(1):10–10, 2007.
- [12] Jonathan Long, Evan Shelhamer, and Trevor Darrell. Fully convolutional networks for semantic segmentation. In *Proceedings of the IEEE conference on computer vision and pattern recognition*, pages 3431–3440, 2015.
- [13] Alex Krizhevsky and Ilya Sutskever. E. hinton, geoffrey.(2012). imagenet classification with deep convolutional neural networks. *Neural Information Processing Systems*, 25(10.1145):3065386, 2012.
- [14] Karen Simonyan and Andrew Zisserman. Very deep convolutional networks for large-scale image recognition. In *3rd International Conference on Learning Representations, ICLR 2015, San Diego, CA, USA, May 7-9, 2015, Conference Track Proceedings*, 2015.
- [15] Christian Szegedy, Wei Liu, Yangqing Jia, Pierre Sermanet, Scott Reed, Dragomir Anguelov, Dumitru Erhan, Vincent Vanhoucke, and Andrew Rabinovich. Going deeper with convolutions. In *2015 IEEE Conference on Computer Vision and Pattern Recognition (CVPR)*, pages 1–9, 2015.
- [16] Olaf Ronneberger, Philipp Fischer, and Thomas Brox. U-net: Convolutional networks for biomedical image segmentation. In *International Conference on Medical image computing and computer-assisted intervention*, pages 234–241. Springer, 2015.
- [17] Vijay Badrinarayanan, Alex Kendall, and Roberto Cipolla. Segnet: A deep convolutional encoder-decoder architecture for image segmentation. *IEEE transactions on pattern analysis and machine intelligence*, 39(12):2481–2495, 2017.
- [18] Hengshuang Zhao, Jianping Shi, Xiaojuan Qi, Xiaogang Wang, and Jiaya Jia. Pyramid scene parsing network. In *Proceedings of the IEEE conference on computer vision and pattern recognition*, pages 2881–2890, 2017.
- [19] Liang-Chieh Chen, Yukun Zhu, George Papandreou, Florian Schroff, and Hartwig Adam. Encoder-decoder with atrous separable convolution for semantic image segmentation. In *Proceedings of the European conference on computer vision (ECCV)*, pages 801–818, 2018.
- [20] Ke Sun, Bin Xiao, Dong Liu, and Jingdong Wang. Deep high-resolution representation learning for human pose estimation. In *CVPR*, 2019.
- [21] Yuhui Yuan, Xilin Chen, and Jingdong Wang. Object-contextual representations for semantic segmentation. In Andrea Vedaldi, Horst Bischof, Thomas Brox, and Jan-Michael Frahm, editors, *Computer Vision – ECCV 2020*, pages 173–190, Cham, 2020. Springer International Publishing.
- [22] Towaki Takikawa, David Acuna, Varun Jampani, and Sanja Fidler. Gated-scnn: Gated shape cnns for semantic segmentation. *ICCV*, 2019.
- [23] Yuhui Yuan, Jingyi Xie, Xilin Chen, and Jingdong Wang. Segfix: Model-agnostic boundary refinement for segmentation. In *European Conference on Computer Vision*, pages 489–506. Springer, 2020.
- [24] Gabriel J. Brostow, Jamie Shotton, Julien Fauqueur, and Roberto Cipolla. Segmentation and recognition using structure from motion point clouds. In *ECCV (1)*, pages 44–57, 2008.
- [25] Marius Cordts, Mohamed Omran, Sebastian Ramos, Timo Rehfeld, Markus Enzweiler, Rodrigo Benenson, Uwe Franke, Stefan Roth, and Bernt Schiele. The cityscapes dataset for semantic urban scene understanding. In *Proceedings of the IEEE conference on computer vision and pattern recognition*, pages 3213–3223, 2016.

- [26] Bolei Zhou, Hang Zhao, Xavier Puig, Sanja Fidler, Adela Barriuso, and Antonio Torralba. Scene parsing through ade20k dataset. In *2017 IEEE Conference on Computer Vision and Pattern Recognition (CVPR)*, pages 5122–5130, 2017.
- [27] Jia Deng, Wei Dong, Richard Socher, Li-Jia Li, Kai Li, and Li Fei-Fei. Imagenet: A large-scale hierarchical image database. In *2009 IEEE conference on computer vision and pattern recognition*, pages 248–255. Ieee, 2009.
- [28] Nahian Siddique, Paheding Sidike, Colin Elkin, and Vijay Devabhaktuni. U-net and its variants for medical image segmentation: theory and applications. *arXiv preprint arXiv:2011.01118*, 2020.
- [29] Ning Xu, Brian Price, Scott Cohen, Jimei Yang, and Thomas S Huang. Deep interactive object selection. In *Proceedings of the IEEE Conference on Computer Vision and Pattern Recognition*, pages 373–381, 2016.
- [30] Nanqing Dong and Eric P Xing. Few-shot semantic segmentation with prototype learning. In *BMVC*, volume 3, 2018.
- [31] Kate Rakelly, Evan Shelhamer, Trevor Darrell, Alyosha A. Efros, and Sergey Levine. Conditional networks for few-shot semantic segmentation. In *6th International Conference on Learning Representations, ICLR, Vancouver, BC, Canada, Workshop Track Proceedings*, 2018.
- [32] Ayyappa Kumar Pambala, Titir Dutta, and Soma Biswas. SML: semantic meta-learning for few-shot semantic segmentation. *CoRR*, abs/2009.06680, 2020.
- [33] Pinzhao Tian, Zhangkai Wu, Lei Qi, Lei Wang, Yinghuan Shi, and Yang Gao. Differentiable meta-learning model for few-shot semantic segmentation. In *The Thirty-Fourth AAAI Conference on Artificial Intelligence, AAAI*, pages 12087–12094. AAAI Press, 2020.
- [34] Amirreza Shaban, Shray Bansal, Zhen Liu, Irfan Essa, and Byron Boots. One-shot learning for semantic segmentation. *Proceedings of the British Machine Vision Conference (BMVC)*, pages 167.1–167.13, 2017.
- [35] Xiaolin Zhang, Yunchao Wei, Yi Yang, and Thomas S. Huang. Sg-one: Similarity guidance network for one-shot semantic segmentation. *IEEE Transactions on Cybernetics*, 50(9):3855–3865, 2020.
- [36] Kaixin Wang, Jun Hao Liew, Yingtian Zou, Daquan Zhou, and Jiashi Feng. Panet: Few-shot image semantic segmentation with prototype alignment. In *Proceedings of the IEEE/CVF International Conference on Computer Vision (ICCV)*, October 2019.
- [37] Chi Zhang, Guosheng Lin, Fayao Liu, Rui Yao, and Chunhua Shen. Canet: Class-agnostic segmentation networks with iterative refinement and attentive few-shot learning. In *Proceedings of the IEEE/CVF Conference on Computer Vision and Pattern Recognition (CVPR)*, June 2019.
- [38] Haochen Wang, Xudong Zhang, Yutao Hu, Yandan Yang, Xianbin Cao, and Xiantong Zhen. Few-shot semantic segmentation with democratic attention networks. In *Computer Vision - ECCV 2020 - 16th European Conference, Glasgow, UK, August 23-28, 2020, Proceedings, Part XIII*, volume 12358 of *Lecture Notes in Computer Science*, pages 730–746. Springer, 2020.
- [39] Chi Zhang, Guosheng Lin, Fayao Liu, Jiushuang Guo, Qingyao Wu, and Rui Yao. Pyramid graph networks with connection attentions for region-based one-shot semantic segmentation. In *Proceedings of the IEEE/CVF International Conference on Computer Vision (ICCV)*, October 2019.
- [40] Boyu Yang, Chang Liu, Bohao Li, Jianbin Jiao, and Qixiang Ye. Prototype mixture models for few-shot semantic segmentation. In *Computer Vision - ECCV 2020 - 16th European Conference, Glasgow, UK, August 23-28, 2020, Proceedings, Part VIII*, volume 12353 of *Lecture Notes in Computer Science*, pages 763–778. Springer, 2020.
- [41] Mary C Potter. Meaning in visual search. *Science*, 187(4180):965–966, 1975.

- [42] Philippe G Schyns and Aude Oliva. From blobs to boundary edges: Evidence for time-and spatial-scale-dependent scene recognition. *Psychological science*, 5(4):195–200, 1994.
- [43] Aude Oliva and Philippe G Schyns. Coarse blobs or fine edges? evidence that information diagnosticity changes the perception of complex visual stimuli. *Cognitive psychology*, 34(1):72–107, 1997.
- [44] Warren S McCulloch and Walter Pitts. A logical calculus of the ideas immanent in nervous activity. *The bulletin of mathematical biophysics*, 5(4):115–133, 1943.
- [45] David E Rumelhart, Geoffrey E Hinton, and Ronald J Williams. Learning representations by back-propagating errors. *nature*, 323(6088):533–536, 1986.
- [46] Frank Rosenblatt. The perceptron: a probabilistic model for information storage and organization in the brain. *Psychological review*, 65(6):386, 1958.
- [47] Min Lin, Qiang Chen, and Shuicheng Yan. Network in network. In *2nd International Conference on Learning Representations, ICLR 2014, Banff, AB, Canada, April 14-16, 2014, Conference Track Proceedings*, 2014.
- [48] Kaiming He, Xiangyu Zhang, Shaoqing Ren, and Jian Sun. Deep residual learning for image recognition. In *Proceedings of the IEEE conference on computer vision and pattern recognition*, pages 770–778, 2016.
- [49] Christian Szegedy, Vincent Vanhoucke, Sergey Ioffe, Jonathon Shlens, and Zbigniew Wojna. Rethinking the inception architecture for computer vision. In *Proceedings of IEEE Conference on Computer Vision and Pattern Recognition*, 2016.
- [50] François Chollet. Xception: Deep learning with depthwise separable convolutions. In *2017 IEEE Conference on Computer Vision and Pattern Recognition (CVPR)*, pages 1800–1807, 2017.
- [51] Yann LeCun, Léon Bottou, Yoshua Bengio, and Patrick Haffner. Gradient-based learning applied to document recognition. *Proceedings of the IEEE*, 86(11):2278–2324, 1998.
- [52] A. Waibel, T. Hanazawa, G. Hinton, K. Shikano, and K.J. Lang. Phoneme recognition using time-delay neural networks. *IEEE Transactions on Acoustics, Speech, and Signal Processing*, 37(3):328–339, 1989.
- [53] David H Hubel and Torsten N Wiesel. Receptive fields, binocular interaction and functional architecture in the cat’s visual cortex. *The Journal of physiology*, 160(1):106, 1962.
- [54] Kunihiro Fukushima, Sei Miyake, and Takayuki Ito. Neocognitron: A neural network model for a mechanism of visual pattern recognition. *IEEE transactions on systems, man, and cybernetics*, 45(5):826–834, 1983.
- [55] Gao Huang, Zhuang Liu, Laurens Van Der Maaten, and Kilian Q Weinberger. Densely connected convolutional networks. In *Proceedings of the IEEE conference on computer vision and pattern recognition*, pages 4700–4708, 2017.
- [56] Gao Huang, Danlu Chen, Tianhong Li, Felix Wu, Laurens van der Maaten, and Kilian Weinberger. Multi-scale dense networks for resource efficient image classification. In *International Conference on Learning Representations*, 2018.
- [57] Qianli Liao and Tomaso Poggio. Bridging the gaps between residual learning, recurrent neural networks and visual cortex. *arXiv preprint arXiv:1604.03640*, 2016.
- [58] Hyeonwoo Noh, Seunghoon Hong, and Bohyung Han. Learning deconvolution network for semantic segmentation. In *Proceedings of the IEEE international conference on computer vision*, pages 1520–1528, 2015.
- [59] G. Lin, A. Milan, C. Shen, and I. Reid. RefineNet: Multi-path refinement networks for high-resolution semantic segmentation. In *CVPR*, July 2017.

- [60] Guosheng Lin, Fayao Liu, Anton Milan, Chunhua Shen, and Ian Reid. Refinenet: Multi-path refinement networks for dense prediction. *IEEE Transactions on Pattern Analysis and Machine Intelligence*, 2019.
- [61] Simon Jégou, Michal Drozdal, David Vazquez, Adriana Romero, and Yoshua Bengio. The one hundred layers tiramisu: Fully convolutional densenets for semantic segmentation. In *2017 IEEE Conference on Computer Vision and Pattern Recognition Workshops (CVPRW)*, pages 1175–1183, 2017.
- [62] Md Amirul Islam, Mrigank Rochan, Neil D. B. Bruce, and Yang Wang. Gated feedback refinement network for dense image labeling. In *Computer Vision and Pattern Recognition (CVPR)*, 2017.
- [63] Kaiming He, Georgia Gkioxari, Piotr Dollár, and Ross Girshick. Mask r-cnn. In *Proceedings of the IEEE international conference on computer vision*, pages 2961–2969, 2017.
- [64] Tsung-Yi Lin, Piotr Dollár, Ross Girshick, Kaiming He, Bharath Hariharan, and Serge Belongie. Feature pyramid networks for object detection. In *Proceedings of the IEEE conference on computer vision and pattern recognition*, pages 2117–2125, 2017.
- [65] Shu Liu, Lu Qi, Haifang Qin, Jianping Shi, and Jiaya Jia. Path aggregation network for instance segmentation. In *Proceedings of the IEEE conference on computer vision and pattern recognition*, pages 8759–8768, 2018.
- [66] Liang-Chieh Chen, George Papandreou, Iasonas Kokkinos, Kevin Murphy, and Alan L. Yuille. Semantic image segmentation with deep convolutional nets and fully connected crfs. In *3rd International Conference on Learning Representations, ICLR 2015, San Diego, CA, USA, May 7-9, 2015, Conference Track Proceedings*, 2015.
- [67] Liang-Chieh Chen, George Papandreou, Iasonas Kokkinos, Kevin Murphy, and Alan L. Yuille. Deeplab: Semantic image segmentation with deep convolutional nets, atrous convolution, and fully connected crfs. *IEEE Transactions on Pattern Analysis and Machine Intelligence*, 40(4):834–848, 2018.
- [68] Liang-Chieh Chen, George Papandreou, Florian Schroff, and Hartwig Adam. Rethinking atrous convolution for semantic image segmentation. *CoRR*, abs/1706.05587, 2017.
- [69] Maoke Yang, Kun Yu, Chi Zhang, Zhiwei Li, and Kuiyuan Yang. Denseaspp for semantic segmentation in street scenes. In *2018 IEEE/CVF Conference on Computer Vision and Pattern Recognition*, pages 3684–3692, 2018.
- [70] Wei Liu, Andrew Rabinovich, and Alexander C. Berg. Parsenet: Looking wider to see better. *CoRR*, abs/1506.04579, 2015.
- [71] Liang-Chieh Chen, Yi Yang, Jiang Wang, Wei Xu, and Alan L. Yuille. Attention to scale: Scale-aware semantic image segmentation. In *2016 IEEE Conference on Computer Vision and Pattern Recognition (CVPR)*, pages 3640–3649, 2016.
- [72] Jun Fu, Jing Liu, Haijie Tian, Yong Li, Yongjun Bao, Zhiwei Fang, and Hanqing Lu. Dual attention network for scene segmentation. In *Proceedings of the IEEE Conference on Computer Vision and Pattern Recognition*, pages 3146–3154, 2019.
- [73] Yuhui Yuan and Jingdong Wang. Ocnet: Object context network for scene parsing. *CoRR*, abs/1809.00916, 2018.
- [74] Hang Zhang, Kristin Dana, Jianping Shi, Zhongyue Zhang, Xiaogang Wang, Amrith Tyagi, and Amit Agrawal. Context encoding for semantic segmentation. In *The IEEE Conference on Computer Vision and Pattern Recognition (CVPR)*, June 2018.
- [75] Xiaolong Wang, Ross Girshick, Abhinav Gupta, and Kaiming He. Non-local neural networks. In *2018 IEEE/CVF Conference on Computer Vision and Pattern Recognition*, pages 7794–7803, 2018.

- [76] Di Lin, Dingguo Shen, Siting Shen, Yuanfeng Ji, Dani Lischinski, Daniel Cohen-Or, and Hui Huang. Zigzagnet: Fusing top-down and bottom-up context for object segmentation. In *2019 IEEE/CVF Conference on Computer Vision and Pattern Recognition (CVPR)*, pages 7482–7491, 2019.
- [77] Fan Zhang, Yanqin Chen, Zhihang Li, Zhibin Hong, Jingtuo Liu, Feifei Ma, Junyu Han, and Errui Ding. Acfnnet: Attentional class feature network for semantic segmentation. In *2019 IEEE/CVF International Conference on Computer Vision (ICCV)*, pages 6797–6806, 2019.
- [78] Hang Zhang, Han Zhang, Chenguang Wang, and Junyuan Xie. Co-occurrent features in semantic segmentation. In *2019 IEEE/CVF Conference on Computer Vision and Pattern Recognition (CVPR)*, pages 548–557, 2019.
- [79] Xiangtai Li, Li Zhang, Ansheng You, Maoke Yang, Kuiyuan Yang, and Yunhai Tong. Global aggregation then local distribution in fully convolutional networks. In *BMVC*, 2019.
- [80] Sungha Choi, Joanne T Kim, and Jaegul Choo. Cars can’t fly up in the sky: Improving urban-scene segmentation via height-driven attention networks. In *Proceedings of the IEEE/CVF Conference on Computer Vision and Pattern Recognition*, pages 9373–9383, 2020.
- [81] Gedas Bertasius, Jianbo Shi, and Lorenzo Torresani. High-for-low and low-for-high: Efficient boundary detection from deep object features and its applications to high-level vision. In *Proceedings of the IEEE International Conference on Computer Vision (ICCV)*, December 2015.
- [82] Liang-Chieh Chen, Jonathan T Barron, George Papandreou, Kevin Murphy, and Alan L Yuille. Semantic image segmentation with task-specific edge detection using cnns and a discriminatively trained domain transform. In *CVPR*, 2016.
- [83] Henghui Ding, Xudong Jiang, Ai Qun Liu, Nadia Magnenat Thalmann, and Gang Wang. Boundary-aware feature propagation for scene segmentation. In *Proceedings of the IEEE/CVF International Conference on Computer Vision (ICCV)*, October 2019.
- [84] Dmitrii Marin, Zijian He, Peter Vajda, Priyam Chatterjee, Sam S. Tsai, Fei Yang, and Yuri Boykov. Efficient segmentation: Learning downsampling near semantic boundaries. In *2019 IEEE/CVF International Conference on Computer Vision, ICCV 2019, Seoul, Korea (South), October 27 - November 2, 2019*, pages 2131–2141. IEEE, 2019.
- [85] Zhuotao Tian, Xin Lai, Li Jiang, Michelle Shu, Hengshuang Zhao, and Jiaya Jia. Generalized few-shot semantic segmentation. *CoRR*, abs/2010.05210, 2020.
- [86] Zhiying Cao, Tengfei Zhang, Wenhui Diao, Yue Zhang, Xiaode Lyu, Kun Fu, and Xian Sun. Meta-seg: A generalized meta-learning framework for multi-class few-shot semantic segmentation. *IEEE Access*, 7:166109–166121, 2019.
- [87] Lizhao Liu, Junyi Cao, Minqian Liu, Yong Guo, Qi Chen, and Mingkui Tan. Dynamic extension nets for few-shot semantic segmentation. In *Proceedings of the 28th ACM International Conference on Multimedia, MM ’20*, page 1441–1449, New York, NY, USA, 2020. Association for Computing Machinery.
- [88] Zhuotao Tian, Hengshuang Zhao, Michelle Shu, Zhicheng Yang, Ruiyu Li, and Jiaya Jia. Prior guided feature enrichment network for few-shot segmentation. *IEEE Transactions on Pattern Analysis and Machine Intelligence*, pages 1–1, 2020.
- [89] Gen Li, Varun Jampani, Laura Sevilla-Lara, Deqing Sun, Jonghyun Kim, and Joongkyu Kim. Adaptive prototype learning and allocation for few-shot segmentation. *CoRR*, abs/2104.01893, 2021.
- [90] Xianghui Yang, Bairun Wang, Xinchu Zhou, Kaige Chen, Shuai Yi, Wanli Ouyang, and Luping Zhou. Brinet: Towards bridging the intra-class and inter-class gaps in one-shot segmentation. In *31st British Machine Vision Conference 2020, BMVC 2020, Virtual Event, UK, September 7-10, 2020*. BMVA Press, 2020.

- [91] Sergey Ioffe and Christian Szegedy. Batch normalization: Accelerating deep network training by reducing internal covariate shift. In *International conference on machine learning*, pages 448–456. PMLR, 2015.
- [92] Vinod Nair and Geoffrey E Hinton. Rectified linear units improve restricted boltzmann machines. In *Icml*, 2010.
- [93] Adam Paszke, Sam Gross, Francisco Massa, Adam Lerer, James Bradbury, Gregory Chanan, Trevor Killeen, Zeming Lin, Natalia Gimelshein, Luca Antiga, Alban Desmaison, Andreas Kopf, Edward Yang, Zachary DeVito, Martin Raison, Alykhan Tejani, Sasank Chilamkurthy, Benoit Steiner, Lu Fang, Junjie Bai, and Soumith Chintala. Pytorch: An imperative style, high-performance deep learning library. In *Advances in Neural Information Processing Systems 32*, pages 8024–8035. Curran Associates, Inc., 2019.
- [94] Herbert Robbins and Sutton Monro. A stochastic approximation method. *The annals of mathematical statistics*, pages 400–407, 1951.
- [95] Yurii E Nesterov. A method for solving the convex programming problem with convergence rate $O(1/k^2)$. In *Dokl. akad. nauk Sssr*, volume 269, pages 543–547, 1983.
- [96] Mark Sandler, Andrew Howard, Menglong Zhu, Andrey Zhmoginov, and Liang-Chieh Chen. Mobilenetv2: Inverted residuals and linear bottlenecks. In *2018 IEEE/CVF Conference on Computer Vision and Pattern Recognition*, pages 4510–4520, 2018.
- [97] Mingxing Tan and Quoc V. Le. Efficientnet: Rethinking model scaling for convolutional neural networks. In *Proceedings of the 36th International Conference on Machine Learning, ICML 2019, 9-15 June 2019, Long Beach, California, USA*, volume 97 of *Proceedings of Machine Learning Research*, pages 6105–6114. PMLR, 2019.
- [98] Ilija Radosavovic, Raj Prateek Kosaraju, Ross Girshick, Kaiming He, and Piotr Dollár. Designing network design spaces. In *Proceedings of the IEEE/CVF Conference on Computer Vision and Pattern Recognition*, pages 10428–10436, 2020.
- [99] jfzhang95. pytorch-deeplab-xception (deeplabv3+ with resnet-101 backbone). <https://github.com/jfzhang95/pytorch-deeplab-xception>.
- [100] stigma0617. Vovnet-deeplabv3 (deeplabv3 with densenet161 backbone). <https://github.com/stigma0617/VoVNet-DeepLabV3>.
- [101] Ke Sun, Yang Zhao, Borui Jiang, Tianheng Cheng, Bin Xiao, Dong Liu, Yadong Mu, Xinggang Wang, Wenyu Liu, and Jingdong Wang. Hrnet-semantic-segmentation. <https://github.com/HRNet/HRNet-Semantic-Segmentation>.
- [102] milesial. Pytorch-unet. <https://github.com/milesial/Pytorch-UNet>.
- [103] Saining Xie, Ross Girshick, Piotr Dollár, Zhuowen Tu, and Kaiming He. Aggregated residual transformations for deep neural networks. In *2017 IEEE Conference on Computer Vision and Pattern Recognition (CVPR)*, pages 5987–5995, 2017.
- [104] Pavel Yakubovskiy. Segmentation models pytorch. https://github.com/qubvel/segmentation_models.pytorch, 2020.
- [105] Ke Sun, Yang Zhao, Borui Jiang, Tianheng Cheng, Bin Xiao, Dong Liu, Yadong Mu, Xinggang Wang, Wenyu Liu, and Jingdong Wang. High-resolution representations for labeling pixels and regions. *CoRR*, abs/1904.04514, 2019.
- [106] Vladislav Sovrasov. flops-counter.pytorch. <https://github.com/sovrasov/flops-counter.pytorch>.
- [107] Alex Kendall. Segnet-tutorial. <https://github.com/alexgkendall/SegNet-Tutorial>.
- [108] Timothy M. Hospedales, Antreas Antoniou, Paul Micaelli, and Amos J. Storkey. Meta-learning in neural networks: A survey. *CoRR*, abs/2004.05439, 2020.

A Appendix

A.1 Cityscapes experiments

A.1.1 Baseline experiments

For ease of visualization, we separate the training plots of ResNet-101, DenseNet-161, HRNet-V2, and U-Net from the data ablation study and combine them with baseline experiments. In Figure 3, we present the training plots of the networks trained on six subsets of training data (T_{2975} , T_{1487} , T_{743} , T_{371} , T_{185} , and T_{92}).

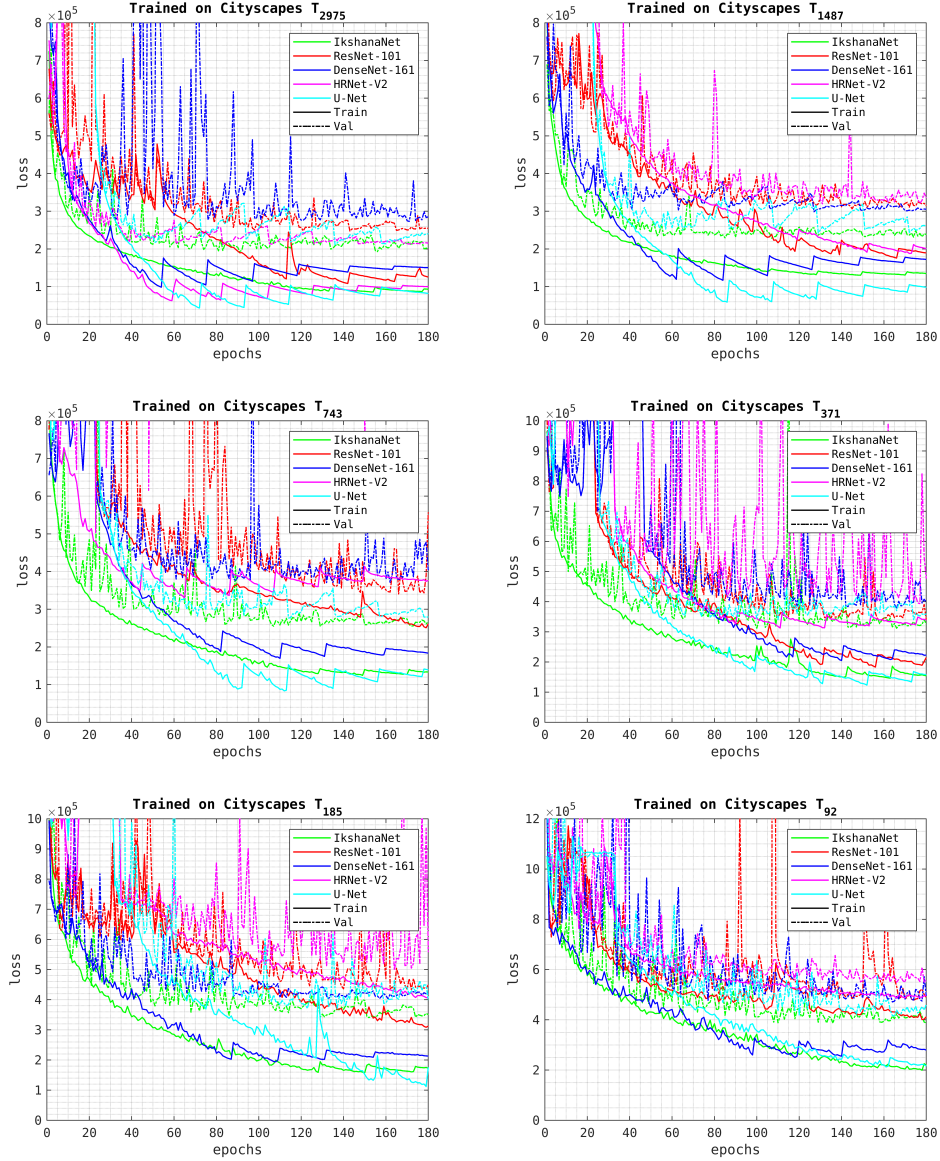


Figure 3: Cityscapes Baseline experiments training plots

A.1.2 Data ablation study

In Figure 4, we present the training plots of the networks Resnet-18, MobileNet-V2, EfficientNet-b1, RegNetY-08, and IkshanaNet-main, trained on five subsets of training data (T_{1487} , T_{743} , T_{371} , T_{185} , and T_{92}). In table 6, we present the class-wise IoU results of these networks.

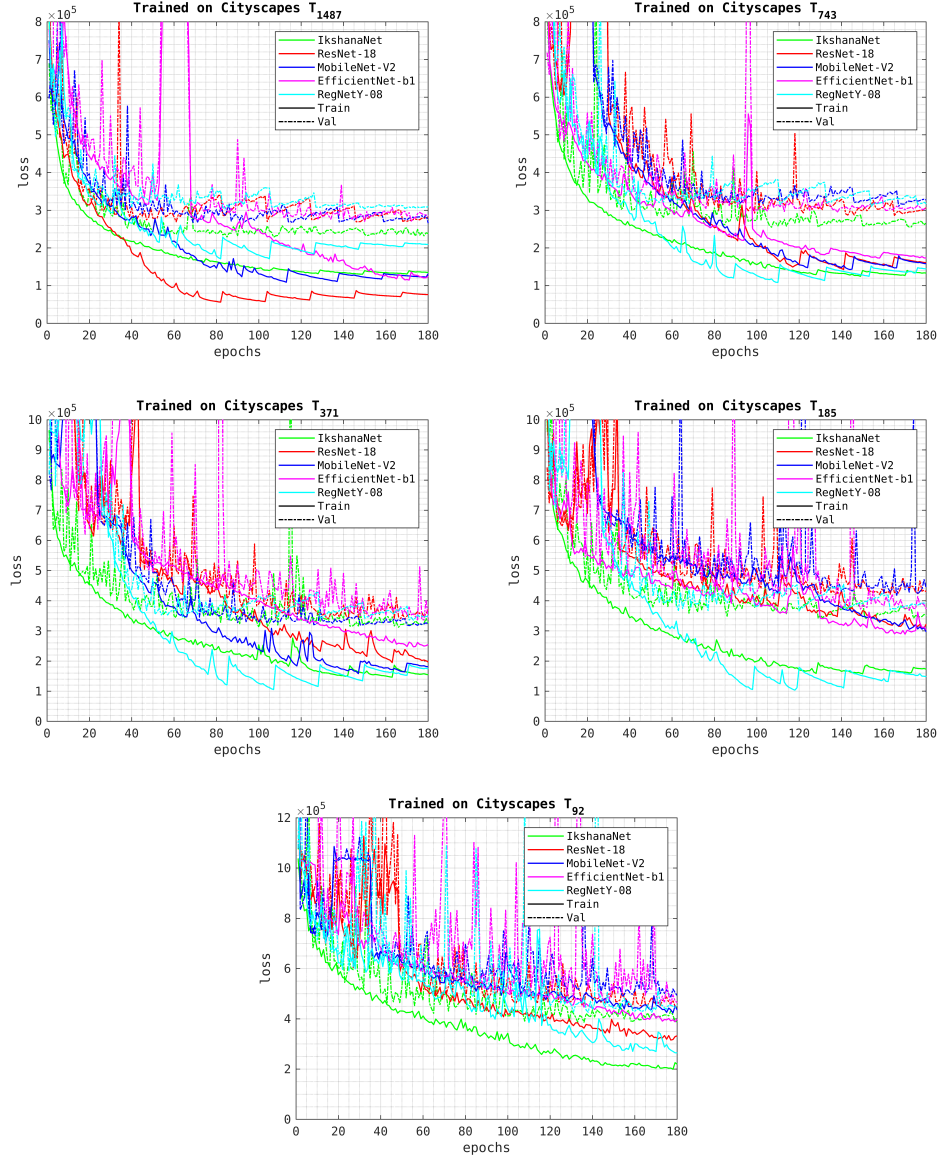


Figure 4: Cityscapes data ablation study training plots

A.1.3 Multi-scale ablation study

In Figure 5, we present the training plots of the networks IkshanaNet-1S-6G, IkshanaNet-2S-3G, and IkshanaNet-3S-2G trained on five subsets of training data (T_{1487} , T_{743} , T_{371} , T_{185} , and T_{92}). In table 7, we present the class-wise IoU results of these networks.

A.2 CamVid experiments

A.2.1 Baseline experiments

In Figure 6, we present the training plots of the networks ResNet-18, EfficientNet-b1, RegNetY-08, MobileNet-V2, and IkshanaNet-3G, trained on three subsets of training data (T_{367} , T_{183} , and T_{91}). In Figure 7, we present the training plots of the networks ResNet-50, EfficientNet-b4, RegNetY-40, ResNext-50, and IkshanaNet-6G, trained on three subsets of training data (T_{367} , T_{183} , and T_{91}). In Figure 8, we present the training plots of the networks ResNet-101, EfficientNet-b6, RegNetY-80,

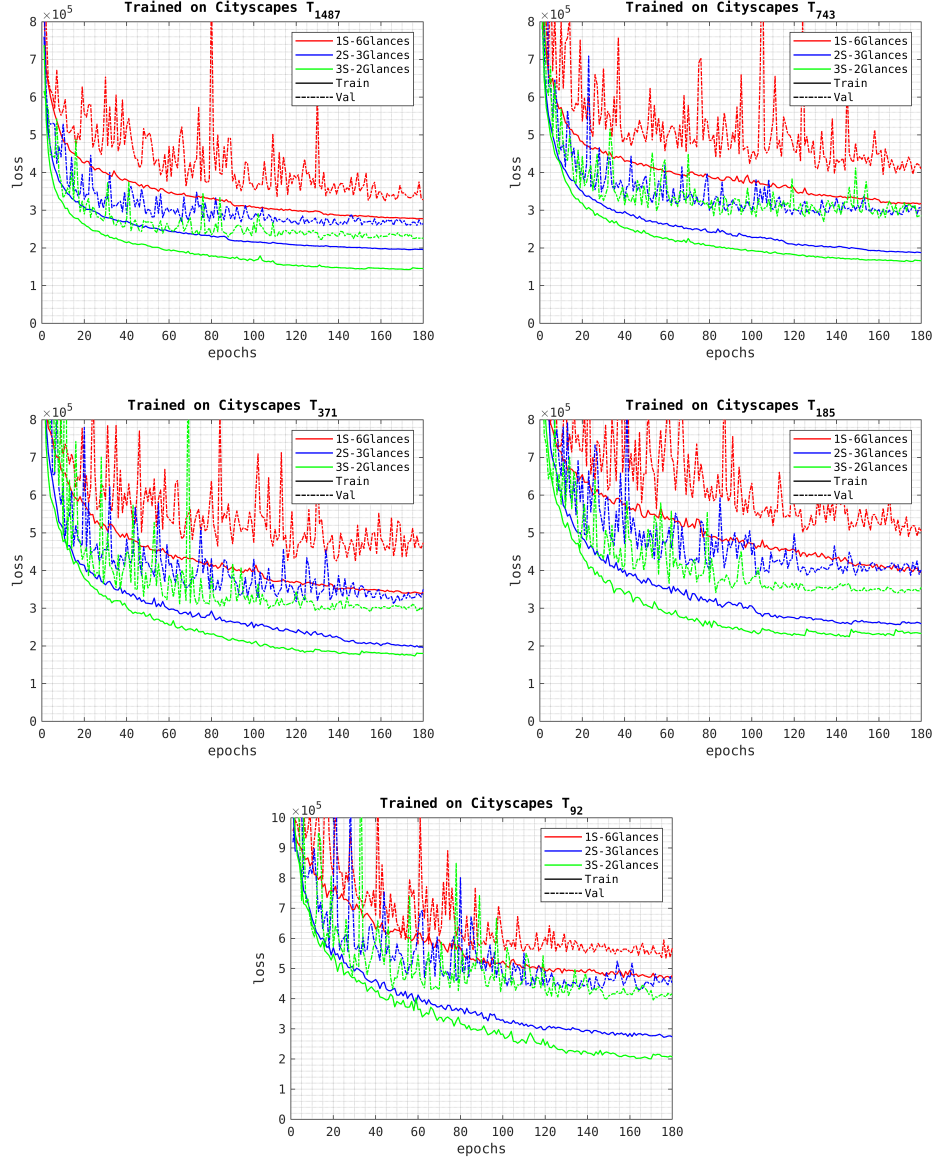


Figure 5: Cityscapes multi-scale ablation study training plots

DenseNet-161, HRNet-V2, U-Net, and IkshanaNet-12G, trained on three subsets of training data (T_{367} , T_{183} , and T_{91}).

A.2.2 Multi-scale ablation study

In Figure 9, we present the training plots of the networks IkshanaNet-1S-6G, IkshanaNet-2S-3G, and IkshanaNet-3S-2G, trained on three subsets of training data (T_{367} , T_{183} , and S_{91}).

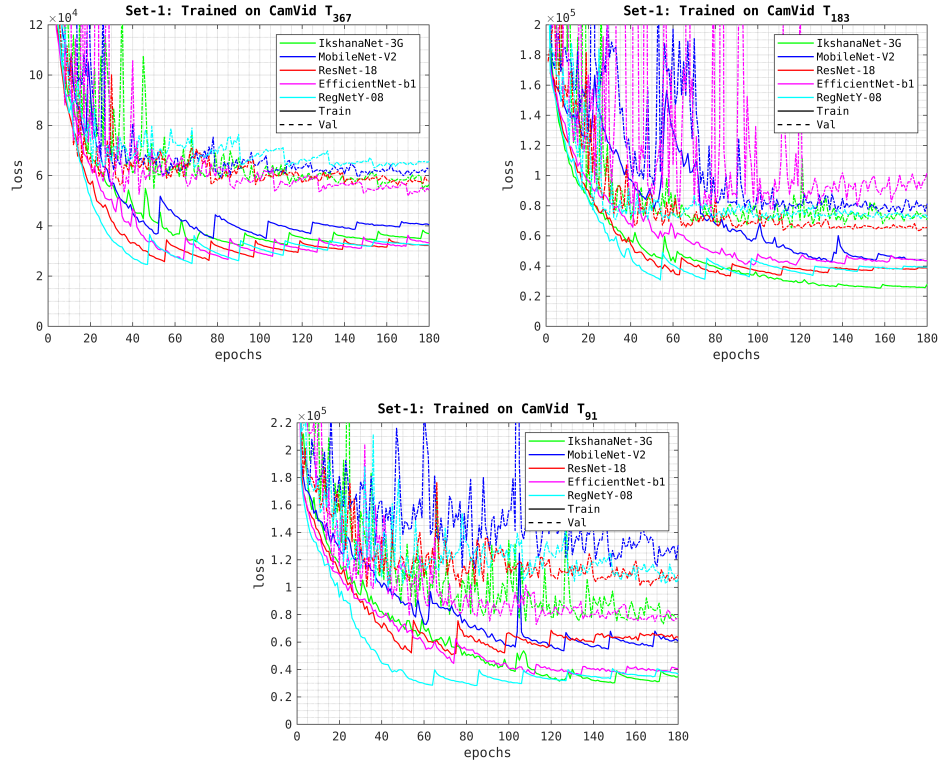


Figure 6: CamVid Set-1 Baseline experiments training plots

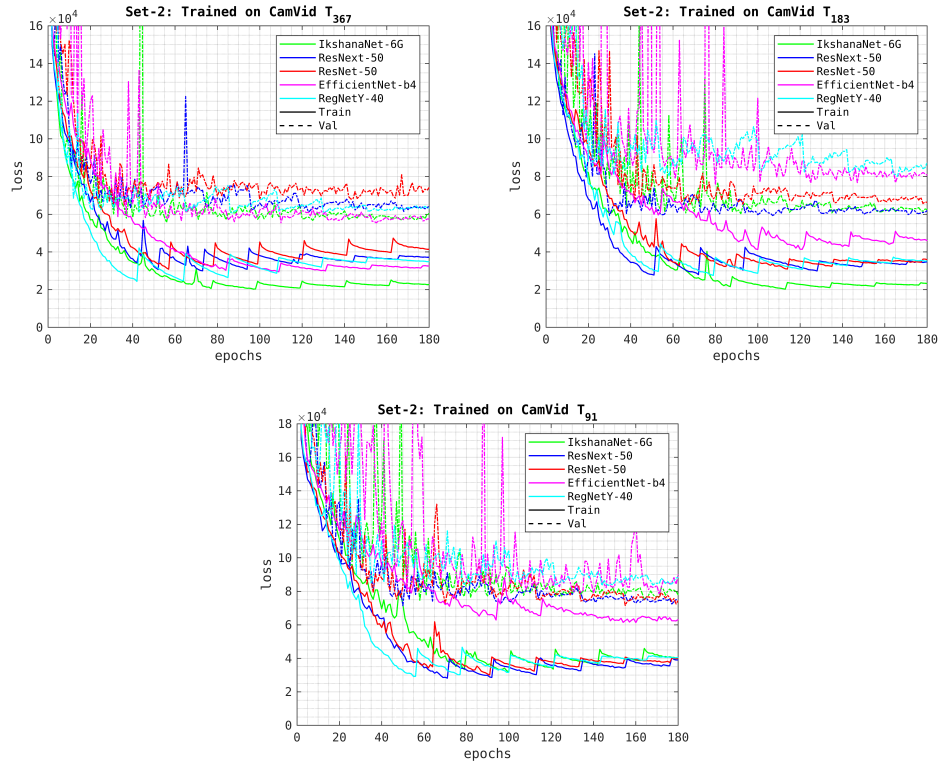


Figure 7: CamVid Set-2 Baseline experiments training plots

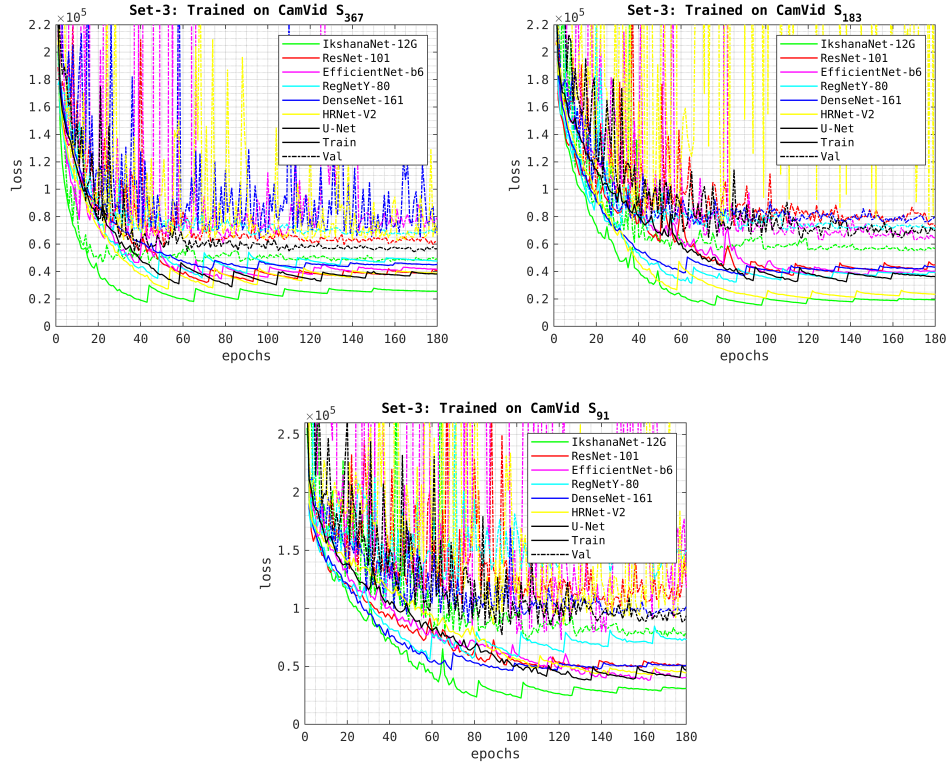


Figure 8: CamVid Set-3 Baseline experiments training plots

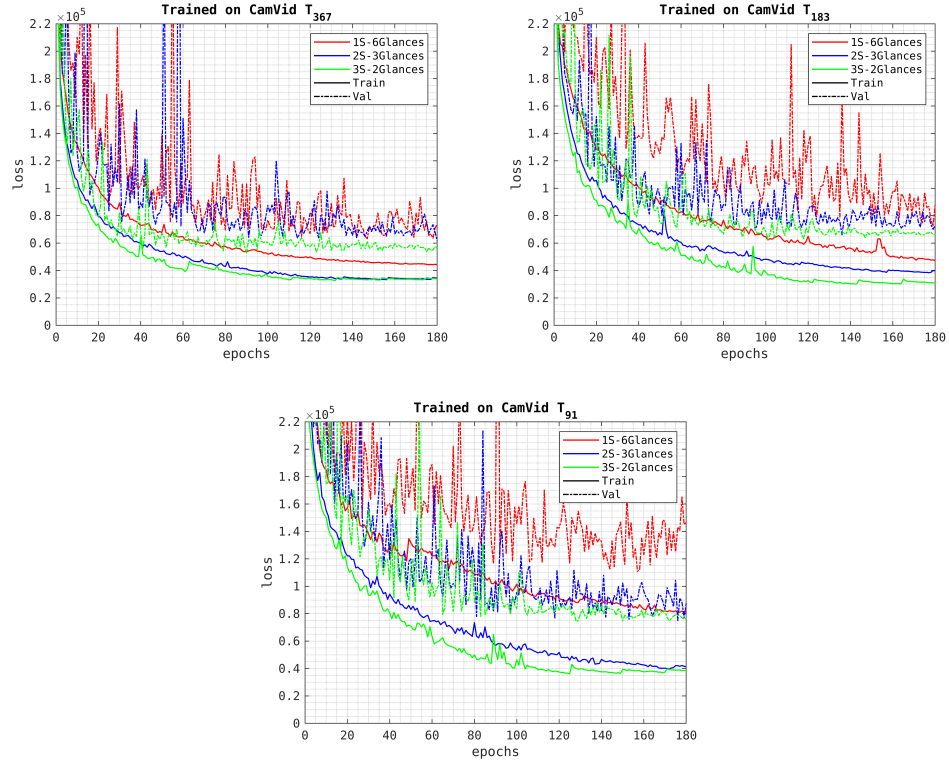


Figure 9: CamVid multi-scale ablation study training plots

		road	sidewalk	building	wall	fence	pole	traffic light	traffic sign	vegetation	terrain	sky	person	rider	car	truck	bus	train	motorcycle	bicycle	Average	
T ₁₄₈₇	ResNet18	93.7	64.4	81.5	14.5	13.8	27.8	17.8	26.3	85.0	46.2	88.8	46.7	7.4	81.3	23.8	34.5	10.1	5.0	39.8	42.6	
	MobileNetV2	93.9	64.6	81.8	15.8	16.2	24.0	1.0	17.6	84.4	39.9	88.6	39.2	0.0	82.5	13.0	26.8	9.0	0.0	32.6	38.5	
	EfficientNetb1	93.3	64.9	81.7	0.3	15.0	26.2	2.5	23.8	83.7	41.4	88.6	42.3	0.0	81.0	0.0	25.7	17.0	0.0	30.7	37.8	
	RegNetY08	94.1	57.7	77.6	0.0	0.3	0.0	0.0	0.0	82.0	41.4	88.4	25.7	0.0	75.0	0.0	0.0	0.0	0.0	0.0	28.5	
	ResNet101-1	93.0	54.0	75.9	12.9	0.9	3.4	0.0	0.2	81.7	38.8	86.9	30.9	0.0	73.7	2.7	0.0	0.0	0.0	1.0	29.3	
	DenseNet161-1	93.1	57.7	78.9	11.2	6.6	11.1	0.0	12.4	81.5	38.3	84.9	35.0	0.0	76.7	13.4	0.3	2.3	0.1	28.3	33.3	
	HRNet-V2	92.3	52.3	76.9	0.7	0.5	0.0	0.0	0.0	81.8	34.5	82.9	9.4	0.0	72.3	0.0	5.3	0.0	0.0	18.6	27.8	
	U-Net	94.0	65.6	83.2	13.9	20.5	34.3	21.7	43.9	87.4	43.1	89.5	49.9	0.0	84.2	12.1	9.9	12.9	0.0	47.9	42.8	
IkshanaNet	93.5	64.7	82.9	17.0	22.6	35.2	27.0	44.1	86.8	41.4	87.2	52.8	2.5	81.5	0.3	25.6	3.9	7.1	48.9	43.4		
T ₇₄₃	ResNet18	92.8	56.3	78.0	15.3	8.0	15.4	4.9	18.9	82.3	42.8	85.6	35.4	0.1	75.2	13.1	13.9	1.9	0.0	36.6	35.6	
	MobileNetV2	92.7	57.3	77.8	6.1	7.8	0.7	0.1	11.3	81.5	39.2	85.2	30.8	0.1	75.9	3.5	22.9	2.9	0.0	15.4	32.2	
	EfficientNetb1	93.5	60.5	77.1	4.1	3.9	9.1	0.0	14.0	81.8	39.6	84.6	22.8	1.6	75.1	9.8	18.6	0.0	0.0	20.8	32.5	
	RegNetY08	93.9	58.7	78.8	3.4	9.1	0.0	0.0	17.5	83.1	45.2	87.1	32.0	0.0	76.8	2.3	0.3	0.0	0.0	17.1	31.9	
	ResNet101	90.5	44.6	72.2	9.2	3.3	5.2	0.0	12.5	79.8	36.2	79.8	25.6	0.0	65.3	0.0	0.0	0.0	0.0	0.0	28.8	
	DenseNet161	91.1	50.8	74.7	13.9	3.3	4.4	1.1	12.1	78.4	32.1	80.8	28.6	0.0	69.6	2.2	1.4	0.2	2.3	25.7	30.1	
	HRNet-V2	86.0	23.6	62.0	0.0	0.0	0.0	0.0	0.0	60.3	10.9	78.1	0.0	0.0	37.3	0.0	0.0	0.0	0.0	0.0	18.8	
	U-Net	93.6	62.1	81.3	5.2	11.6	19.3	0.4	28.1	86.0	42.3	87.8	36.5	0.0	79.6	9.6	0.5	0.0	0.0	5.5	34.2	
IkshanaNet	93.0	60.3	81.4	13.4	23.0	36.5	21.9	42.8	86.3	35.1	87.8	42.5	0.0	80.0	0.1	20.2	0.1	0.7	38.4	40.2		
T ₃₇₁	ResNet18	88.4	46.5	73.5	2.6	1.1	4.0	0.0	5.3	78.4	36.4	82.9	27.9	0.0	68.5	0.0	0.0	0.0	1.4	13.1	27.9	
	MobileNetV2	91.4	50.2	75.2	10.1	7.3	5.6	0.3	8.5	81.0	34.6	83.0	27.8	0.0	72.7	16.0	1.4	0.0	0.0	0.0	16.6	30.6
	EfficientNetb1	89.8	46.4	72.4	5.3	4.9	7.6	0.3	6.5	75.7	32.7	77.3	20.7	0.0	65.1	0.0	0.0	0.0	0.0	6.8	26.9	
	RegNetY08	91.6	50.5	76.3	10.3	5.8	0.0	0.3	10.3	81.2	38.3	84.5	26.2	0.0	70.6	8.1	0.0	0.0	0.0	3.8	29.4	
	ResNet101	89.2	45.8	73.6	9.8	2.7	3.1	0.0	8.0	79.9	34.8	81.6	26.9	0.0	65.3	8.9	0.0	0.0	0.0	13.8	28.6	
	DenseNet161	89.0	42.4	71.9	8.1	2.1	0.0	0.0	0.3	75.7	33.8	77.4	18.6	0.0	64.3	3.3	0.2	0.0	0.0	6.2	26.0	
	HRNet-V2	87.4	35.3	68.7	0.1	0.0	0.0	0.0	0.0	74.7	33.9	76.4	8.9	0.0	56.2	0.0	0.0	0.0	0.0	0.3	23.3	
	U-Net	92.3	57.4	76.9	4.7	7.4	2.7	1.2	14.1	83.4	36.6	85.8	28.5	0.0	75.8	3.3	0.0	1.9	0.0	1.4	30.2	
IkshanaNet	90.5	51.6	78.1	4.5	1.7	28.0	0.7	24.0	84.0	33.4	83.9	35.2	0.0	65.5	0.1	0.8	0.0	0.0	20.3	31.7		
T ₁₈₅	ResNet18	85.0	32.3	70.4	1.6	0.0	0.0	0.0	0.0	75.9	32.0	75.2	0.0	0.0	53.0	0.0	0.0	0.0	0.0	0.0	22.4	
	MobileNetV2	85.9	37.3	68.8	0.0	0.0	0.0	0.0	0.0	74.1	34.6	71.3	0.0	0.0	54.6	0.0	0.0	0.0	0.0	0.0	22.5	
	EfficientNetb1	85.2	38.8	71.0	4.1	1.5	0.0	0.0	0.2	78.6	31.8	80.0	17.9	0.0	58.1	0.0	0.0	0.0	0.0	0.0	24.6	
	RegNetY08	89.4	47.2	74.3	6.5	2.5	0.0	0.2	8.2	78.9	35.7	82.6	22.4	0.0	66.9	3.1	0.0	0.0	0.0	2.2	27.4	
	ResNet101	85.4	29.7	66.9	0.0	0.0	0.0	0.0	0.0	73.4	31.3	75.0	0.0	0.0	48.5	0.0	0.0	0.0	0.0	0.0	21.6	
	DenseNet161	87.8	40.2	72.2	3.2	2.4	0.0	0.0	0.0	76.9	28.3	78.6	15.2	0.0	61.5	2.3	0.0	0.0	0.0	5.1	24.9	
	HRNet-V2	86.4	19.3	63.8	0.0	0.0	0.0	0.0	0.0	67.9	0.0	70.6	0.0	0.0	38.8	0.0	0.0	0.0	0.0	0.0	18.3	
	U-Net	90.2	50.1	74.0	7.5	0.6	0.0	0.0	8.1	81.1	33.1	82.7	13.2	0.0	68.4	0.0	0.0	0.6	0.2	18.4	27.8	
IkshanaNet	90.1	49.2	74.6	5.9	3.8	17.7	2.0	18.7	81.6	33.6	80.7	29.6	0.0	66.9	3.2	0.0	0.0	0.0	10.2	29.9		
T ₉₂	ResNet18	85.7	26.4	66.4	0.0	0.0	0.0	0.0	0.0	74.2	26.9	72.9	0.0	0.0	47.4	0.0	0.0	0.0	0.0	0.0	21.0	
	MobileNetV2	82.1	20.4	63.7	0.0	0.0	0.0	0.0	0.0	69.2	25.5	67.7	0.0	0.0	36.6	0.0	0.0	0.0	0.0	0.0	19.2	
	EfficientNetb1	84.7	26.6	59.8	1.6	0.0	0.0	0.0	0.1	67.2	29.9	58.6	2.4	0.0	46.1	0.0	0.0	0.0	0.0	0.0	19.8	
	RegNetY08	86.7	33.4	68.5	0.0	0.0	0.0	0.0	0.0	74.8	27.9	76.3	0.0	0.0	52.8	0.0	0.0	0.0	0.0	0.0	22.1	
	ResNet101	81.4	20.7	62.2	0.0	0.0	0.0	0.0	0.0	69.4	28.2	68.6	0.0	0.0	39.9	0.0	0.0	0.0	0.0	0.0	19.4	
	DenseNet161	84.0	24.3	67.5	0.0	0.3	0.0	0.0	0.0	72.7	23.0	74.6	0.0	0.0	49.3	0.0	0.0	0.0	0.0	0.0	20.8	
	HRNet-V2	81.0	3.2	49.5	0.0	0.0	0.0	0.0	0.0	52.0	0.0	67.2	0.0	0.0	38.9	0.0	0.0	0.0	0.0	0.0	15.4	
	U-Net	87.6	45.8	71.3	2.2	0.0	0.0	0.0	5.8	79.2	31.1	79.8	14.2	0.0	58.4	0.0	0.0	0.3	0.0	0.0	25.0	
IkshanaNet	87.0	40.0	72.3	3.0	3.2	10.4	0.0	2.3	79.3	31.3	79.1	20.8	0.0	58.9	0.0	0.0	0.0	0.0	2.9	25.8		

Table 6: Class-wise results of the Cityscapes data ablation study evaluated on val set

Subset	Method	road	sidewalk	building	wall	fence	pole	traffic light	traffic sign	vegetation	terrain	sky	person	rider	car	truck	bus	train	motorcycle	bicycle	Average
S_{1487}	1S-6Glances	86.0	44.5	72.2	4.0	3.3	21.9	2.0	28.0	83.1	35.4	77.5	29.7	0.0	52.8	0.0	0.9	0.0	0.0	12.7	29.2
	2S-3Glances	90.9	57.5	78.6	9.0	13.8	34.6	16.8	42.8	85.3	39.9	83.7	42.2	0.0	73.1	0.0	5.4	0.2	0.0	35.0	37.3
	3S-2Glances	94.0	67.6	83.0	16.4	24.7	39.1	23.7	47.1	87.0	41.7	87.9	50.7	2.2	81.1	3.6	18.7	5.4	2.8	49.6	43.5
S_{743}	1S-6Glances	85.0	34.0	67.6	0.2	0.3	17.1	0.6	15.4	80.4	30.0	74.8	20.9	0.0	45.2	0.0	0.0	0.0	0.0	1.4	24.9
	2S-3Glances	90.8	56.8	77.4	8.6	13.3	31.6	12.6	33.6	85.8	38.1	84.1	38.3	0.0	66.9	0.1	0.0	0.0	0.1	24.3	34.9
	3S-2Glances	92.3	60.5	80.0	11.2	14.7	31.6	6.2	33.6	85.5	39.7	86.8	41.4	0.0	73.9	4.6	2.3	6.8	2.1	28.8	36.9
S_{371}	1S-6Glances	80.6	29.4	65.1	1.0	0.3	8.8	1.5	8.8	79.0	27.7	73.8	22.3	0.0	43.9	0.0	0.0	0.0	0.0	1.1	23.0
	2S-3Glances	88.6	51.4	74.3	5.9	10.4	26.1	0.9	28.3	83.8	36.5	82.7	37.3	0.0	66.7	0.6	6.3	2.4	0.0	28.8	33.2
	3S-2Glances	90.7	56.0	78.1	12.0	12.0	26.8	4.5	26.1	83.6	33.6	85.4	38.5	0.0	70.7	3.8	3.5	0.0	0.2	27.6	34.4
S_{185}	1S-6Glances	80.0	18.2	59.1	0.0	0.0	6.0	0.2	2.9	73.3	26.0	72.0	8.6	0.0	35.7	0.8	0.0	0.0	0.0	0.0	20.2
	2S-3Glances	84.8	39.5	69.3	3.6	0.4	7.8	0.0	12.8	78.8	32.7	79.9	19.3	0.0	52.0	0.0	0.0	0.0	0.0	8.0	25.7
	3S-2Glances	88.7	43.4	72.9	1.5	3.7	12.9	0.2	12.7	81.1	31.5	80.0	24.9	0.0	61.6	2.2	0.0	0.0	0.0	4.4	27.5
S_{92}	1S-6Glances	77.7	11.1	52.5	0.0	0.0	0.0	0.1	3.6	71.7	25.0	70.5	1.9	0.0	30.5	0.0	0.0	0.0	0.0	0.0	18.1
	2S-3Glances	82.7	32.9	66.5	2.4	0.1	8.7	0.0	10.9	78.0	29.1	76.7	18.8	0.0	46.8	0.0	0.0	0.1	0.0	2.0	24.0
	3S-2Glances	86.8	34.6	71.6	4.5	6.6	8.3	0.0	10.8	79.5	32.7	78.0	24.7	0.0	59.5	0.3	0.0	0.0	0.0	5.0	26.5